Lithuanian Journal of Physics, Vol. **56**, No. 3, pp. 173–181 (2016)

STRAIN ENGINEERING OF ELECTRICAL CONDUCTIVITY IN EPITAXIAL THIN $Ba_{0.7}Sr_{0.3}TiO_3$ FILM HETEROSTRUCTURES

R. Mackevičiūtė [a], Š. Bagdzevičius [a], M. Ivanov [a], B. Fraygola [b], R. Grigalaitis [a], N. Setter [b], and J. Banys [a]

[a] *Faculty of Physics, Vilnius University, Saulėtekio 9, LT-10222 Vilnius, Lithuania*
[b] *Ceramics Laboratory, Swiss Federal Institute of Technology (EPFL), CH-1015 Lausanne, Switzerland*
E-mail: ruta.mackeviciute@ff.vu.lt

Received 5 February 2016; revised 1 March 2016; accepted 21 June 2016

Thin epitaxial films have a great potential to be used in real life applications, such as oxide-on-silicon. However, they often contain a large amount of defects, leading to an enhanced electrical conductivity. This could be desirable in some applications (i. e. memristors), but the mechanism is not fully understood. Here we report on the investigation of epitaxial barium strontium titanate thin films deposited on strontium titanate single crystal substrates ($Ba_{0.7}Sr_{0.3}TiO_3/SrRuO_3//SrTiO_3$ heterostructures) with a controlled epitaxial strain. The impedance analysis allowed us to propose a model, which explains changes in the temperature dependence of the conductivity based on the strain-dependent anisotropic change of electron/hole mobility.

Keywords: thin films, impedance spectroscopy, electron mobility, ferroelectrics

PACS: 77.55.-g, 84.37.+g, 73.50.Gr, 77.80.B-

1. Introduction

Barium strontium titanate ($Ba_{1-x}Sr_xTiO_3$, hereafter referred to as BST) thin films have been intensively investigated for applications in high density dynamic random access memories [1], IR detection [2], tunable microwave devices [3], and also for the sensing of humidity [4, 5] and gas [6]. The material is very attractive for engineers because of its high dielectric constant, low dielectric loss, good thermal stability, and good high frequency characteristics. BST is a continuous solid solution between $BaTiO_3$ and $SrTiO_3$ over the whole concentration range. Both experimental reports and theoretical studies of the BST phase diagram of single crystals and ceramic were published in a number of papers [7–12]. It was shown that the temperatures of all three phase transitions of pure barium titanate decrease linearly in the BST solid solution with increasing of the Sr content up to $0.2 < x < 0.25$. In this solid solution region all phase transitions merge into one and the paraelectric–ferroelectric phase transition type transforms from the first order to the second order one [10]. As a result, the transition temperature and hence the electrical and optical properties of BST ceramic can be tuned in a controllable way to get various functionalities for electronic and electromechanical applications.

While it is possible to tailor properties of the bulk material by changing its chemical composition, thin films add one more way for fine-tuning the properties – internal fields. They could be, in most cases, electrical, mechanical or both. These fields arise due to a variety of reasons including the lattice mismatch between the film and the substrate in the case of epitaxial films and differences between the thermal expansion coefficients (TECs) of the film and the substrate [13]. The lattice mismatch is known to alter the Curie temperature, leading to the stabilisation of the ferroelectric phase at much higher temperatures [13]. However, these effects are much more visible in epitaxial thin films, while interfacial effects are most significant in the case of polycrystalline films. The interfaces often contain depleted regions [14] as perovskite oxide ferroelectrics are wide-bandgap semiconductors [15]. This leads to the formation of the so-called "dead layer", which significantly deteriorates the macroscopically observable properties [16, 17]. Epitaxial films would be beneficial in the cases of real devices as there would be only one well-defined interface. Unfortunately, the leakage current in epitaxial thin films is often very high, and its origin is not fully understood. It is agreed that at room temperature (RT) perovskites (in contrary to non-oxide covalent semiconductors like Si) contain large concentrations of defects [18], oxygen vacancies being most probable of

them [19, 20]. Migration of these defects and reorientation of the extended defect complexes [21–23] play a key role in resistance degradation and fatigue of ferroelectric ceramic capacitors and devices. Similar effects take place at the micro- and nanoscale in the thin films and are responsible for the long-term degradation of properties [24, 25]. However, little is known about the exact origin of the defects and mechanisms of charge transfer. The aim of this work is to link the misfit strain of the film with mobility, or rather its activation energy, of the most abundant charge carriers.

2. Experiment

$Ba_{0.7}Sr_{0.3}TiO_3$ (BST) epitaxial thin films of different thicknesses were deposited by the pulsed laser deposition technique (PLD with RHEED – reflection high energy electron diffraction – capability) using a KrF excimer laser (λ = 248 nm) on (001) oriented low miscut $SrTiO_3$ (STO) single-crystalline substrates (*CrysTec*, Germany). $SrRuO_3$ (SRO) was used as a lower electrode in the metal–insulator–metal structure. Prior to the heterostructure deposition, STO substrates were etched in buffered HF acid (buffered oxide etchant) and annealed (in O_2 flow) at high temperature (approx. 1 hour at 900 °C) according to the procedure described in the work of Koster et al. [26] to obtain a single site terminated and atomically smooth surface. BST and SRO layers were deposited from ceramic targets on the STO substrates at 800 and 625 °C temperatures, respectively, 0.143–0.146 mbar partial oxygen pressure in the deposition chamber, 32–40 mJ laser energy and 2–3 Hz repetition rate. After the depositions, all samples with the BST and SRO films were annealed in a PLD chamber (to assure oxygen stoichiometry) at increased partial oxygen pressure (p_{O_2} was increased from 0.145 mbar to 1 mbar) while cooling down from the deposition temperature. The cooling rate was 10 °C/min.

XRD experiments (coupled ω–2Θ and rocking curve – ω scans) were performed at room temperature with a *Bruker* D8 Discover high resolution diffractometer using a Ni filtered monochromatic Cu K_α radiation source. The epitaxial relations and thickness of thin films were measured after the deposition by TEM (*Philips* CM300 FEG TEM operated at 300 kV). Local piezoelectric characterization at room temperature was done with an *Asylum Research* Cypher AFM piezoelectric force microscope (PFM) working in the DART (dual AC surface resonance tracking and band excitation mode) enhanced sensitivity mode [27] with Ti/Ir or Cr/Pt coated conductive probes.

An HP4284 precision LCR-meter was used for the complex impedance measurements at temperatures from 500 to 300 K during the cooling cycle at a rate of about 1 K/min and frequencies from 20 to 1 MHz. Before the electrical measurements sputtered Pt or Cr/Au top electrodes were deposited through a shadow mask. In this article we will use the abbreviations BST 215 and BST 160 which correspond to $Ba_{0.7}Sr_{0.3}TiO_3$ thin films with the thickness of the functional layer equal to 215 and 160 nm, respectively.

3. Experimental results

Figure 1 shows the frequency dependences of specific impedance of 215 and 160 nm films. A strong

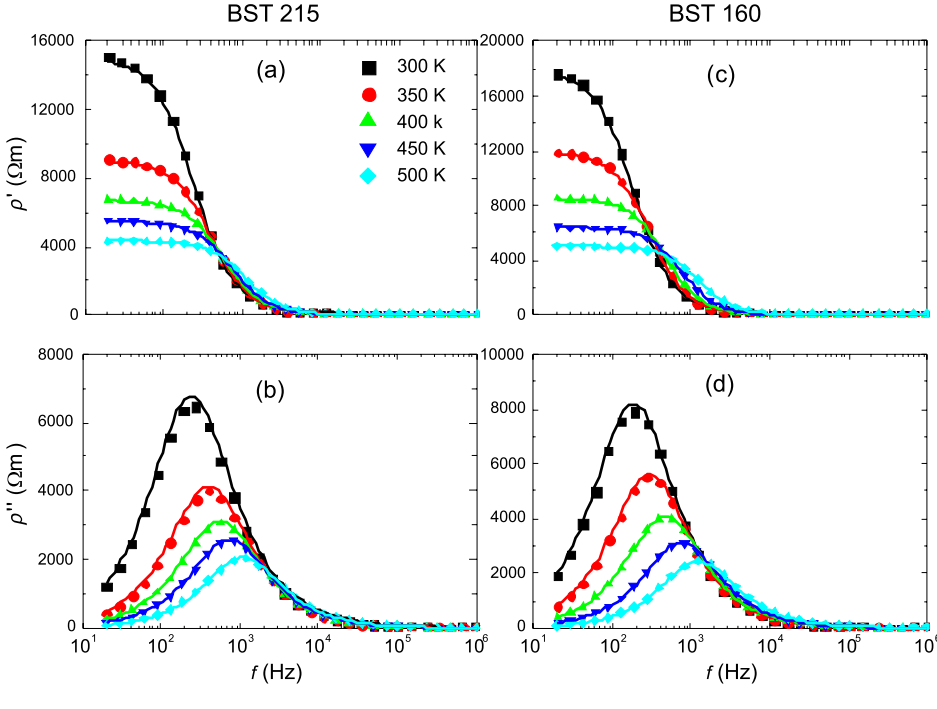

Fig. 1. Frequency dependences of the real ((a) and (c)) and imaginary ((b) and (d)) parts of the specific resistivity of 215 and 160 nm BST films, respectively. Solid lines represent the fits with Eq. (1).

dispersion of specific resistivity can be seen below ~10 kHz frequency for both samples. On cooling the maximum of the imaginary part of ρ^* moves toward lower frequencies indicating the thermally stimulated behaviour of this dispersion. To gain more information from this dispersion we fitted it to the Havriliak–Negami equation [28] which generalises all relaxation-type dispersion relations:

$$\rho^* = \frac{\Delta\rho}{(1+(\mathrm{i}\omega\tau)^{1-\alpha})^{\gamma}}. \quad (1)$$

Here $\Delta\rho$ corresponds to the static specific resistivity, τ is the mean relaxation time of the process, α describes the spectral width, and γ is related to both the spectral width and asymmetry. ω is the angular frequency. During the data approximation it was found that α and γ parameters differ by less than 0.05 from 0 and 1, respectively. Thus, if one replaces these parameters in Eq. (1) by the respective constant values, we arrive at the situation where our system can be described as a single parallel RC circuit.

The values of dielectric permittivity, which were recalculated from the complex resistivity data, are presented in Fig. 2. Experimental investigations of the phase diagram of BST crystals [8], supported by theoretical calculations [9], have shown that the addition of Sr to $BaTiO_3$ leads to the decrease of temperatures of all three phase transitions and at 30 percent of strontium doping the ferroelectricity appears slightly below the room temperature. In the case of thin films, substrate-induced stress shifts the ferroelectric phase transition to higher temperatures when compared to the bulk material [13]. Indeed, in Fig. 2 the dielectric anomaly can be observed at somewhat higher (approx. 400 K) temperature but only at the highest frequencies. While it does not resemble the real peak of the dielectric permittivity at the phase transition point, it could be that this peak is blurred due to high electrical conductivity. As it is clearly seen from Figs. 2(b) and (d), low frequency dielectric losses are really high and screen completely the dielectric response. Another reason could be the weakening of the ferroelectric properties due to the size effect. In nanosized materials it is often the case [29]. It could be that in our films we have the superposition of both effects.

BST in both heterostructures was in the ferroelectric phase at room temperature. This fact was confirmed by the possibility to write an artificial ferroelectric domain pattern into the heterostructure by PFM (Fig. 3).

XRD measurements of 215 and 160 nm thick samples are presented in Fig. 4. STO, SRO and BST peaks are clearly distinguishable and indexed in both heterostructures. In the both cases SRO and BST layers were epitaxially deposited, evidenced by the STO having only <001> family diffraction peaks, and the corresponding SRO_{pc} and BST showing only (00l) diffraction peaks. We have indexed the SRO as having pseudo cubic lattice symmetry – SRO_{pc}; this is usually a sufficient approximation when the SRO film is fully strained and serves only as an electrode, but not as

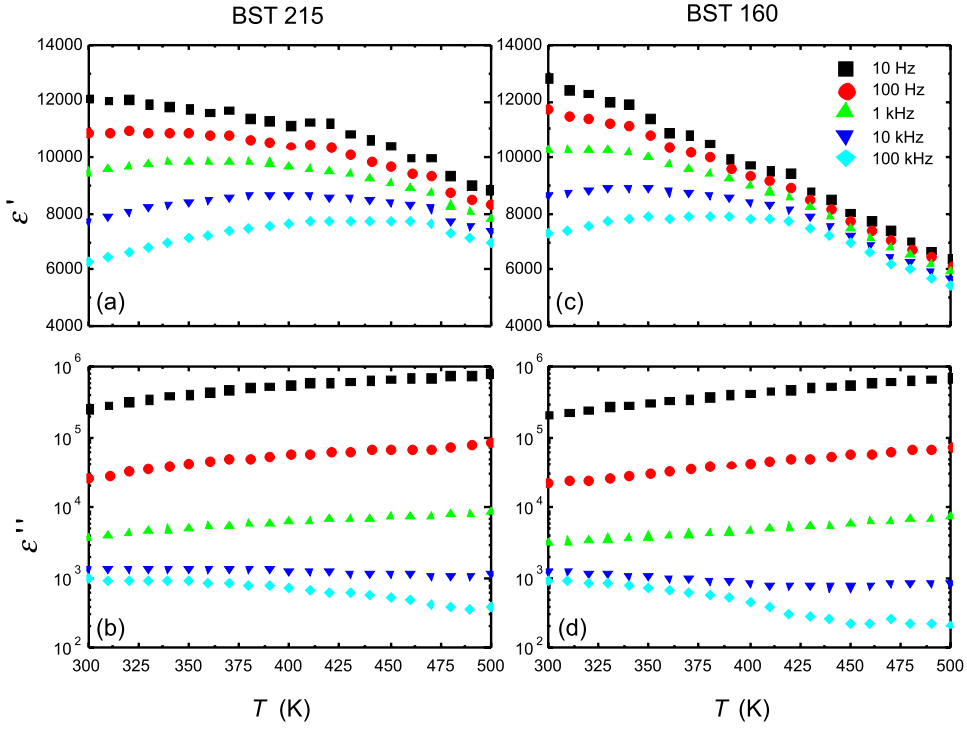

Fig. 2. Temperature dependences of the real ((a) and (c)) and imaginary ((b) and (d)) parts of the dielectric permittivity of 215 and 160 nm BST films.

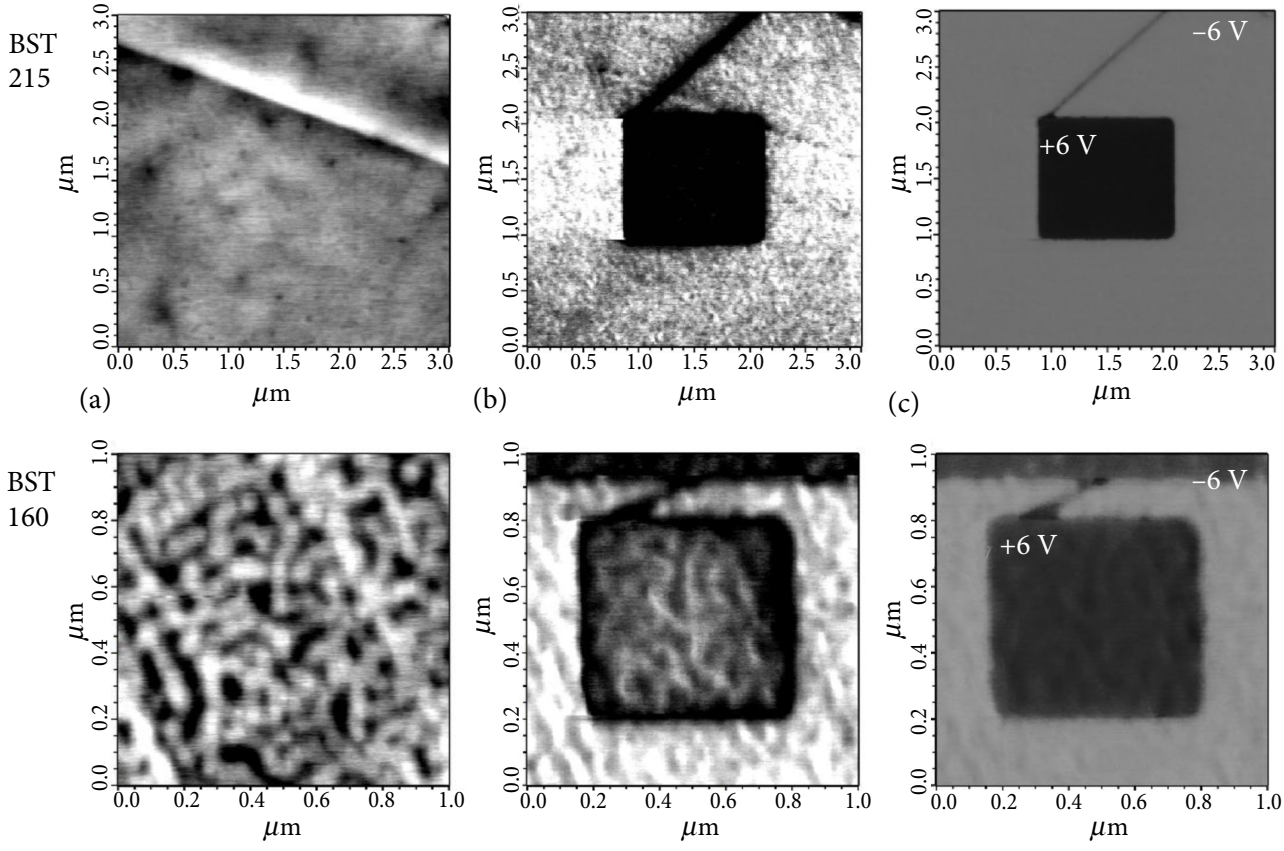

Fig. 3. PFM DART images of the artificially written ferroelectric domain patterns in BST 215 and BST 160 samples. (a) Topography (1.1 nm height difference for BST 215 and 1.2 nm for BST 160), (b) PFM amplitude (370 pm amplitude difference for BST 215 and 420 pm for BST 160), and (c) phase (more than 180° difference for both samples), after the poling experiment with – and + 6 V. Voltage applied to the SRO lower electrode and the PFM cantilever was grounded, negative voltage was applied to all scan area, then positive voltage was applied to a small square, finally imaged without DC bias.

a strain relaxation layer. No secondary phases or differently oriented grains were observed by XRD (large angle scans are not shown here). Out-of-plane lattice parameters of BST and SRO_{pc} were elongated due to the presence of epitaxial strain and clamping by the underneath STO lattice. For the SRO layer, the strain arose from mismatches of the lattice parameter and thermal expansion coefficient compared to the substrate. For the BST layer, there was an additional strain component due to the ferroelectric phase

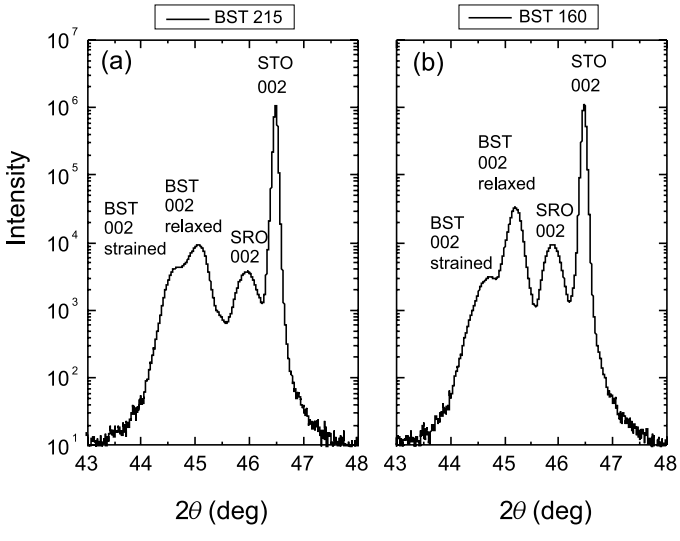

Fig. 4. X-ray diffraction (ω–2Θ scan) patterns of (a) 215 and (b) 160 nm films.

transformation at T_c (ferroelectric phase transition from cubic/paraelectric to tetragonal/ferroelectric phases in bulk material), evidenced as formation of an *a*/*c* ferroelastic/ferroelectric domain pattern below T_c (Fig. 5 left).

In the 215 nm heterostructure, the BST 002 peak is split into a double peak at 44.63 and 45.06° (44.71 and 45.2° in BST 160 case). Such splitting can be related to the differently oriented *a* and *c* ferroelectric (and ferroelastic) domains (with different out of plane lattice parameters) or an unintentionally formed BST bilayer – two separated sublayers with different relaxation state and defect densities. The unavoidable strain relaxation in thick enough epilayers (thicker than critical thickness [30]) and probable formation of two sublayers, also observed by other researchers in similar BST/SRO//STO heterostructures [31], was chosen as the most probable scenario in our work. No splitting of the BST (002) peak was observed in thinner films even with *a*/*c* ferroelastic domain patterns (Fig. 5). The formation of two BST sublayers is due to the change of the film growth mode, from a perfectly coherent (to substrate) lattice (probably step-flow mode) without any dislocations, to a less coherent one, with considerable strain relaxation (2D growth mode). Unfortunately, the transition between these two growth modes was not observed by RHEED, most likely due to fast roughening of the film surface and transition to the 3D (island) mode (also observed in [31]).

In the 160 nm film, the diffraction intensity of the relaxed part is much higher than that of the strained part (absolute intensity differs more than 10 times). The intensity must be proportional to the volume. This indicates that almost all thin film is relaxed. On the other hand, the thicker film has two distinct regions with different strain, which give similar diffraction intensity and, correspondingly, volume.

Unequal volume fractions of strained and relaxed sublayers (in different thickness BST films) are confirmed by reciprocal temperature dependences of the static specific resistivity, which are plotted in Fig. 6. These graphs show the Arrhenius-type behaviour, therefore the experimental data was fitted to Eq. (2) (solid lines in the figure):

$$\Delta\rho = \rho_0 e^{E_a/kT}. \tag{2}$$

Here ρ_0 is the specific resistivity at infinite temperature, *Ea* is the activation energy, and *T* is the temperature.

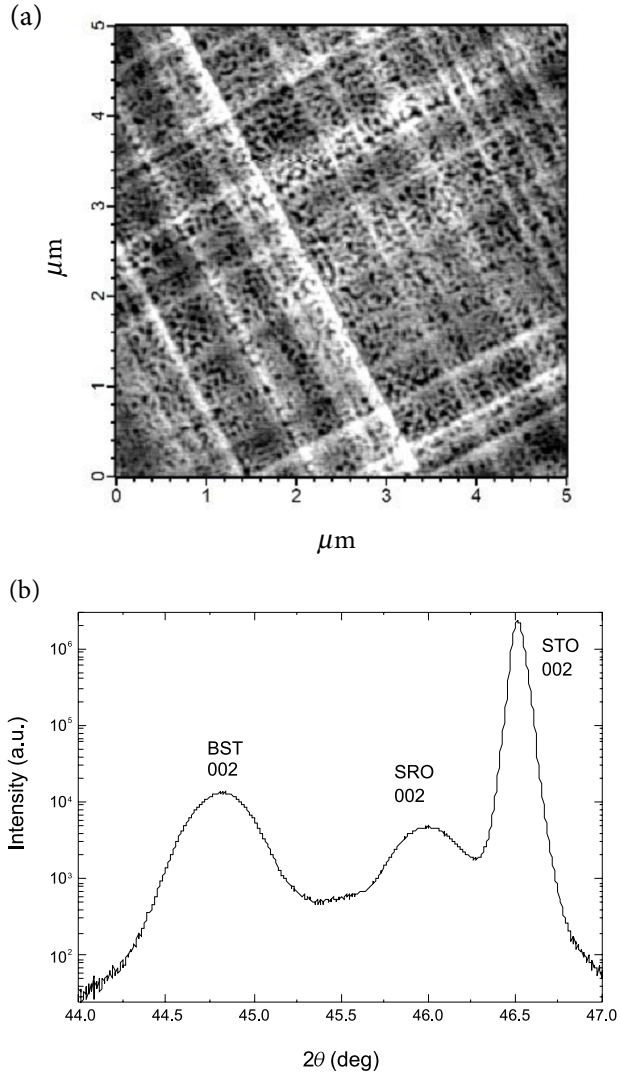

Fig. 5. PFM topography (a) (1.4 nm height difference) with a dense *a*/*c* ferroelastic domain pattern and an XRD ω–2Θ curve (b) of the same sample. No BST peak splitting is observed.

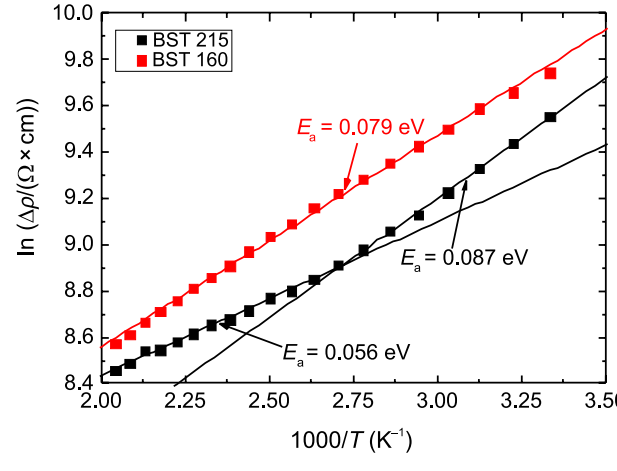

Fig. 6. Reciprocal temperature dependence of the static specific resistivity of thin BST films.

It was found that the 160 nm thick film has a single section with activation energy of 0.079 eV. Meanwhile, the 215 nm thick film has two regions with different activation energies: 0.056 above and 0.087 eV below the 370 K temperature. This can be explained by the (non-) uniform strain of the films. Below we propose a model to explain the results.

Let us assume that a thin film consists of a bottom electrode, a top electrode and two functional layers (strained and relaxed) as shown in Fig. 7.

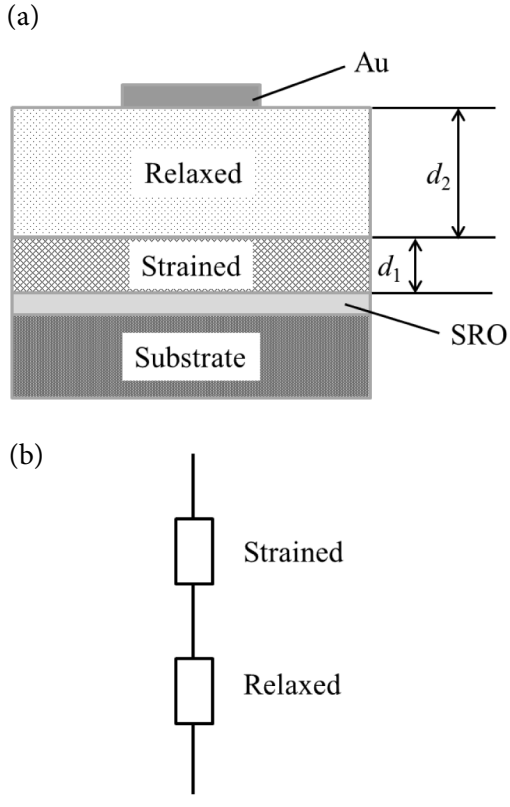

Fig. 7. Schematic illustration of a double layered thin film (a) and its equivalent circuit (b).

In the case of the 215 nm film the two layers are of roughly the same thickness, while in the other case one of the layers (the relaxed one) is much thicker than the other. For example, in the case of the 215 nm film, layer thicknesses can be assumed to be roughly equal to $d_1 = d_2 = 100$, and in the case of 160 nm film, $d_1 = 10$ and $d_2 = 150$ nm.

We can rewrite the Arrhenius law for electrical resistance of each functional layer:

$$R_{\text{strained}} = \rho_1 \cdot \frac{d_1}{S} \cdot \exp\left(\frac{E_1}{kT}\right),$$

$$R_{\text{strained}} = \rho_2 \cdot \frac{d_2}{S} \cdot \exp\left(\frac{E_2}{kT}\right).$$

Here S is the area of the top electrode.

The total sample resistance is equal to a sum of the resistances of the strained and relaxed functional layers, as it is equivalent to the series connection of the layers (Fig. 7(b)):

$$R = R_{\text{strained}} + R_{\text{relaxed}}.$$

In such a case, the biggest resistance will dominate the total resistance, and the experimentally observed value of the activation energy will be determined by the activation energy of the dominating resistance.

A schematic illustration of the reciprocal temperature dependence of the total electrical resistance of double layered thin films is presented in Fig. 8. Here, vertical black dashed lines show an experimental temperature range. Red and black solid lines represent the total resistance of the films with 160 and 215 nm thicknesses, respectively. This illustration indicates that both samples exhibit the same behaviour. In the case of the 160 nm film, the resistance of the strained layer dominates at much higher temperatures than in the case of the 215 nm sample, thus the change of activation energy is visible only in the latter case.

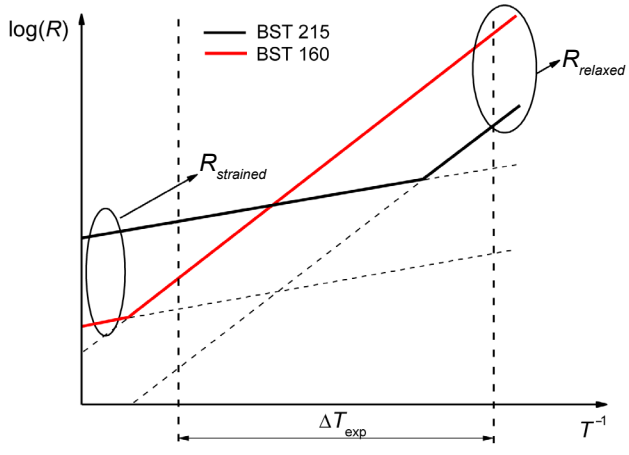

Fig. 8. Schematic illustration of reciprocal temperature dependence of electrical resistance of double layered thin films. Solid lines (red and black online) represent the total resistance of the sample, while short-dashed lines are resistances of the uniform layers.

This model allows us to associate the activation energies with strain in the layers. It is possible due to the fact that both samples are fabricated with the same deposition parameters except the deposition time, which was needed to alter the total thickness. Thus, the nature of defects (and the source of electrons or holes) in the samples can be expected to be the same.

The dependence of activation energy on strain in thin BST films was calculated according to the relation $(c_f–c_b)/c_f$ where c_f and c_b are the out-of-plane lattice constants of the film and bulk material, respectively. The lattice constants for our films have been obtained from X-ray measurements and c_b was taken from the literature [32]. The results of the calculations are presented in Table 1.

Table 1. Dependence of the activation energy on the out-of-plane strain in thin BST films of various thicknesses.

Film thickness	Strain, %		Activation energy, meV	
	Strained	Relaxed	Strained	Relaxed
160 nm	1.38	0.33	–	79±0.86
215 nm	1.56	0.65	56±1.12	87±1.23

As we can see from Table 1, the activation energies of relaxed layers in different films are different. The BST layers were deposited at the same PLD conditions but at different strain state at deposition temperature. The strain state depends on the density of dislocations at deposition temperature. The latter depends on the thickness of the layer [33], which was varied. As a result, different concentration of defects (dopants) in different samples was obtained even though the deposition conditions were the same, as evident from different activation energies for the relaxed layers. However, the activation energy of the specific resistivity is inversely proportional to the strain of the film if all other parameters (i. e. dopant concentration) are the same. This is easily realised in the case of physically the same film, which is in BST 215. Furthermore, the concentration of possible structural defects is smaller in the strained layers, since relaxation is realised by defects, i. e. displacement of ions. This means that bigger activation energy in the case of a relaxed layer can only be related to strain. Keeping in mind the low values of E_a, the conductivity must be coming from some easily ionised defects, which are the source of either electrons or holes. However, the activation energy of the resistivity depends on the ionisation energy of the defects (which is unlikely to change as drastically with strain) as well as the activation energy of the electron/hole mobility. Furthermore, the induced strain must be creating an anisotropic environment around the defects. This would lead to anisotropic mobility of the charge carriers. As the investigated films are epitaxial and the resistivity was measured in the out-of-plane geometry, this means that the positive out-of-plane strain lowers the activation energy of mobility, leading to the decrease in the activation energy of specific resistivity.

4. Conclusions

We have reported on the synthesis and experimental investigation of electrical properties of epitaxial BST 70/30 thin films grown on the (001) STO substrate. It was found that the films consist of two BST sublayers, one of them fully strained by the substrate and the other relaxed. These layers have different activation energies of the specific resistivity. A model was proposed to explain the experimental results, which points to an important conclusion – the positive out-of-plain strain lowers the activation energy of the mobility of electrons (or holes) in the investigated films. The obtained results can be used to engineer the mobility of charge carriers in thin films by strain in various electronic devices, such as memristors, electromechanical devices and on-chip resistors in oxide-on-Si integrated circuits.

Acknowledgements

This work has been financed by the Lithuanian–Swiss Cooperation Program to Reduce Economic and Social Disparities within the Enlarged European Union, Joint Research Project "SLIFE", Project Code No. CH-3-ŠMM-01/02.

References

[1] A.I. Kingon, J.-P. Maria, and S.K. Streiffer, Alternative dielectrics to silicon dioxide for memory and logic devices, Nature **406**(6799), 1032–1038 (2000), http://dx.doi.org/10.1038/35023243

[2] H. Zhu, J. Miao, M. Noda, and M. Okuyama, Preparation of BST ferroelectric thin film by metal organic decomposition for infrared sensor, Sensors Actuators A Phys. **110**(1–3), 371–377 (2004), http://dx.doi.org/10.1016/j.sna.2003.10.074

[3] M. Jain, S.B. Majumder, R.S. Katiyar, and A.S. Bhalla, Novel barium strontium titanate $Ba_{0.5}Sr_{0.5}TiO_3$/MgO thin film composites for tunable microwave devices, Mater. Lett. **57**(26–27), 4232–4236 (2003), http://dx.doi.org/10.1016/S0167-577X(03)00296-9

[4] S. Agarwal, G.L. Sharma, and R. Manchanda, Electrical conduction in (Ba, Sr)TiO_3 thin film MIS capacitor under humid conditions, Solid State Commun. **119**(12), 681–686 (2001), http://dx.doi.org/10.1016/S0038-1098(01)00284-8

[5] S. Agarwal and G.L. Sharma, Humidity sensing properties of (Ba, Sr) TiO_3 thin films grown by hydrothermal–electrochemical method, Sensors Actuators B Chem. **85**(3), 205–211 (2002), http://dx.doi.org/10.1016/S0925-4005(02)00109-0

[6] W. Zhu, O.K. Tan, Q. Yan, and J.T. Oh, Microstructure and hydrogen gas sensitivity of

amorphous (Ba, Sr)TiO_3 thin film sensors, Sensors Actuators B Chem. **65**(1–3), 366–370 (2000), http://dx.doi.org/10.1016/S0925-4005(99)00402-5

[7] F. Jona and G. Shirane, *Ferroelectric Crystals* (Dover Publications, New York, 1993).

[8] L. Benguigui, Disordered ferroelectrics: $Ba_xSr_{1-x}TiO_3$ single crystals, Phys. Status Solidi A **46**(1), 337–342 (1978), http://dx.doi.org/10.1002/pssa.2210460144

[9] V.B. Shirokov, V.I. Torgashev, A.A. Bakirov, and V.V. Lemanov, Concentration phase diagram of $Ba_xSr_{1-x}TiO_3$ solid solutions, Phys. Rev. B **73**(10), 104116 (2006), http://dx.doi.org/10.1103/PhysRevB.73.104116

[10] V.V. Lemanov, E.P. Smirnova, P.P. Syrnikov, and E.A. Tarakanov, Phase transitions and glass-like behavior in $Sr_{1-x}Ba_xTiO_3$, Phys. Rev. B **54**(5), 3151–3157 (1996), http://dx.doi.org/10.1103/PhysRevB.54.3151

[11] C. Ménoret, J.M. Kiat, B. Dkhil, M. Dunlop, H. Dammak, and O. Hernandez, Structural evolution and polar order in $Sr_{1-x}Ba_xTiO_3$, Phys. Rev. B **65**(22), 224104 (2002), http://dx.doi.org/10.1103/PhysRevB.65.224104

[12] E.P. Smirnova, A.V. Sotnikov, R. Kunze, M. Weihnacht, O.E. Kvyatkovskii, and V.V. Lemanov, Interrelation of antiferrodistortive and ferroelectric phase transitions in $Sr_{1-x}A_xTiO_3$ (A=Ba, Pb), Solid State Commun. **133**(7), 421–425 (2005), http://dx.doi.org/10.1016/j.ssc.2004.12.016

[13] Z.-G. Ban and S.P. Alpay, Phase diagrams and dielectric response of epitaxial barium strontium titanate films: A theoretical analysis, J. Appl. Phys. **91**(11), 9288–9296 (2002), http://dx.doi.org/10.1063/1.1473675

[14] W. Känzig, Space charge layer near the surface of a ferroelectric, Phys. Rev. **98**(2), 549–550 (1955), http://dx.doi.org/10.1103/PhysRev.98.549

[15] I. Grinberg, D.V. West, M. Torres, G. Gou, D.M. Stein, L. Wu, G. Chen, E.M. Gallo, A.R. Akbashev, P.K. Davies, J.E. Spanier, and A.M. Rappe, Perovskite oxides for visible-light-absorbing ferroelectric and photovoltaic materials, Nature **503**(7477), 509–512 (2013), http://dx.doi.org/10.1038/nature12622

[16] P. Papet, J.P. Dougherty, and T.R. Shrout, Particle and grain size effects on the dielectric behavior of the relaxor ferroelectric $Pb(Mg_{1/3}Nb_{2/3})O_3$, J. Mater. Res. **5**(12), 2902–2909 (1990), http://dx.doi.org/10.1557/JMR.1990.2902

[17] M.H. Frey, Z. Xu, P. Han, and D.A. Payne, The role of interfaces on an apparent grain size effect on the dielectric properties for ferroelectric barium titanate ceramics, Ferroelectrics **206**(1), 337–353 (1998), http://dx.doi.org/10.1080/00150199808009168

[18] H.L. Tuller and S.R. Bishop, Point defects in oxides: tailoring materials through defect engineering, Annu. Rev. Mater. Res. **41**(1), 369–398 (2011), http://dx.doi.org/10.1146/annurev-matsci-062910-100442

[19] R.A. De Souza, V. Metlenko, D. Park, and T.E. Weirich, Behavior of oxygen vacancies in single-crystal $SrTiO_3$: Equilibrium distribution and diffusion kinetics, Phys. Rev. B **85**(17), 174109 (2012), http://dx.doi.org/10.1103/PhysRevB.85.174109

[20] R. Meyer, R. Waser, J. Helmbold, and G. Borchardt, Observation of vacancy defect migration in the cation sublattice of complex oxides by ^{18}O tracer experiments, Phys. Rev. Lett. **90**(10), 105901 (2003), http://dx.doi.org/10.1103/PhysRevLett.90.105901

[21] R. Waser, T. Baiatu, and K.-H. Härdtl, DC electrical degradation of perovskite-type titanates: I, ceramics, J. Am. Ceram. Soc. **73**(6), 1645–1653 (1990), http://dx.doi.org/10.1111/j.1151-2916.1990.tb09809.x

[22] M. Morozov, D. Damjanovic, and N. Setter, The nonlinearity and subswitching hysteresis in hard and soft PZT, J. Eur. Ceram. Soc. **25**(12), 2483–2486 (2005), http://dx.doi.org/10.1016/j.jeurceram-soc.2005.03.086

[23] K. Carl and K.H. Hardtl, Electrical after-effects in Pb(Ti, Zr)O_3 ceramics, Ferroelectrics **17**(1), 473–486 (1977), http://dx.doi.org/10.1080/00150197808236770

[24] M. Grossmann, S. Hoffmann, S. Gusowski, R. Waser, S.K. Streiffer, C. Basceri, C.B. Parker, S.E. Lash, and A.I. Kingon, Resistance degradation behavior of $Ba_{0.7}Sr_{0.3}TiO_3$ thin films compared to mechanisms found in titanate ceramics and single crystals, Integr. Ferroelectr. **22**(1–4), 83–94 (1998), http://dx.doi.org/10.1080/10584589808208032

[25] W.L. Warren, D. Dimos, G.E. Pike, B.A. Tuttle, M.V. Raymond, R. Ramesh, and J.T. Evans Jr., Voltage shifts and imprint in ferroelectric capacitors, Appl. Phys. Lett. **67**(6), 866–868 (1995), http://dx.doi.org/10.1063/1.115531

[26] G. Koster, B.L. Kropman, G.J.H.M. Rijnders, D.H.A. Blank, and H. Rogalla, Quasi-ideal strontium titanate crystal surfaces through formation of strontium hydroxide, Appl. Phys. Lett. **73**(20), 2920–2922 (1998), http://dx.doi.org/10.1063/1.122630

[27] B.J. Rodriguez, C. Callahan, S.V. Kalinin, and R. Proksch, Dual-frequency resonance-tracking atomic force microscopy, Nanotechnology **18**(47), 475504 (2007), http://dx.doi.org/10.1088/0957-4484/18/47/475504

[28] S. Havriliak and S. Negami, A complex plane analysis of α-dispersions in some polymer systems, J. Polym. Sci. Polymer Sci. Part C **14**(1), 99–117 (1966), http://dx.doi.org/10.1002/polc.5070140111

[29] Z. Zhao, V. Buscaglia, M. Viviani, M.T. Buscaglia, L. Mitoseriu, A. Testino, M. Nygren, M. Johnsson, and P. Nanni, Grain-size effects on the ferroelectric behavior of dense nanocrystalline $BaTiO_3$ ceramics, Phys. Rev. B **70**(2), 024107 (2004), http://dx.doi.org/10.1103/PhysRevB.70.024107

[30] J.W. Matthews and A.E. Blakeslee, Defects in epitaxial multilayers: I. Misfit dislocations, J. Cryst. Growth **27**, 118–125 (1974), http://dx.doi.org/10.1016/S0022-0248(74)80055-2

[31] J.Q. He, E. Vasco, C.L. Jia, R. Dittmann, and R.H. Wang, Microstructure of epitaxial $Ba_{0.7}Sr_{0.3}TiO_3$/$SrRuO_3$ bilayer films on $SrTiO_3$ substrates, J. Appl. Phys. **97**(10), 104907 (2005), http://dx.doi.org/10.1063/1.1897067

[32] Y. Fan, S. Yu, R. Sun, L. Li, Y. Yin, K.-W. Wong, and R. Du, Microstructure and electrical properties of Mn-doped barium strontium titanate thin films prepared on copper foils, Appl. Surf. Sci. **256**(22), 6531–6535 (2010), http://dx.doi.org/10.1016/j.apsusc.2010.04.042

[33] P.-E. Janolin, A.S. Anokhin, Z. Gui, V.M. Mukhortov, Y.I. Golovko, N. Guiblin, S. Ravy, M.E. Marssi, Y.I. Yuzyuk, L. Bellaiche, and B. Dkhil, Strain engineering of perovskite thin films using a single substrate, J. Phys. Condens. Matter **26**(29), 292201 (2014), http://dx.doi.org/10.1088/0953-8984/26/29/292201

ĮTEMPIAIS VALDOMAS ELEKTRINIS LAIDUMAS EPITAKSINĖSE $Ba_{0,7}Sr_{0,3}TiO_3$ PLONŲJŲ SLUOKSNIŲ HETEROSTRUKTŪROSE

R. Mackevičiūtė [a], Š. Bagdzevičius [a], M. Ivanov [a], B. Fraygola [b], R. Grigalaitis [a], N. Setter [b], J. Banys [a]

[a] *Vilniaus universiteto Fizikos fakultetas, Vilnius, Lietuva*

[b] *Šveicarijos federalinis technologijos institutas (EPFL), Lozana, Šveicarija*

Santrauka

Plonieji epitaksiniai sluoksniai yra patrauklūs įvairiems komerciniams taikymams, pavyzdžiui, silicio lustams su integruotomis oksidų heterostruktūromis. Deja, defektų koncentracija juose dažniausiai būna didelė, o tokie sluoksniai – elektriškai laidūs. Tai gali būti naudinga kai kuriems taikymams (pvz., memristoriuose), tačiau pats laidumo mechanizmas nėra iki galo suprastas. Straipsnyje pateikiame epitaksinių plonųjų bario stroncio titanato sluoksnių ant kristalinio stroncio titanato padėklo ($Ba_{0.7}Sr_{0.3}TiO_3$/$SrRuO_3$//$SrTiO_3$ heterostruktūros) tyrimus kontroliuojant epitaksinius įtempimus. Remiantis elektrinės pilnutinės varžos analize, pateiktas teorinis modelis, paaiškinantis temperatūrinę elektrinio laidumo elgseną įtempimų sukeltu anizotropiniu elektronų / skylių judrio kitimu.